RESEARCH ARTICLE

An experimental optimization system for rare mutation detection based on digital PCR droplet clustering analysis and multi-task learning

Zhi He*, Yi Yuan, Jie Wang

School of Medical Technology, Luohe Medical College, Luohe, Henan, China.

Received: April 1, 2026; **accepted:** July 22, 2026.

Rare mutation detection is a critical technology in cancer diagnosis and treatment. Although digital polymerase chain reaction (dPCR) has been widely applied in this field, its performance is often affected by operator-defined parameters and limited clinical adaptability. The detection of rare mutations frequently requires extensive testing, while droplet-level result interpretation in dPCR assays remains highly sensitive to parameter settings. dPCR faces challenges in accommodating diverse clinical scenarios and integrating into routine diagnostic and therapeutic workflows. This study developed an experimental optimization system that integrated droplet clustering with multitask learning (MTL) to achieve both droplet classification and coordinated parameter optimization. The system extracted multidimensional droplet fluorescence intensity feature vectors, droplet fluorescence area signal-to-noise ratio feature vectors, fluorescence decay coefficients, and droplet circularity features. The extracted features were standardized and processed within MTL framework to enable joint optimization of two tasks. A constrained K-means algorithm and an adaptive loss function were further incorporated to enhance model performance. The results demonstrated that the proposed system achieved a detection sensitivity of 97.2%, a specificity of 98.5%, and a clustering accuracy of 96.8%. These metrics significantly outperformed those of commercial software and conventional algorithms. The system also exhibited excellent stability and generalization across different clinical samples, detection platforms, and mutation sites with coefficients of variation ranging from only 0.8% to 1.2%. By addressing key limitations of conventional dPCR approaches, the proposed system provided valuable technical support for the standardized clinical application of dPCR and precision cancer detection.

Keywords: digital PCR; clustering analysis; multi-task learning; rare mutations; mutation detection.

***Corresponding author:** Zhi He, School of Medical Technology, Luohe Medical College, Luohe, Henan 462000, China. Email: hezhixj@126.com.

Introduction

Accurate detection of rare mutations is a core technology for early cancer screening, evaluation of drug-resistance mechanisms, and therapeutic efficacy assessment. The sensitivity and specificity of mutation detection directly affect the accuracy of clinical decision-making [1]. Digital polymerase chain reaction (dPCR), which enables single-molecule detection, has become the gold-standard technology for rare mutation analysis [2]. In dPCR, nucleic acid samples are partitioned into tens of thousands to millions of independent droplets. Mutation quantification is then achieved through parallel amplification and fluorescence signal interpretation. Droplet clustering analysis represents a critical step in this process because it distinguishes positive, negative, and invalid droplets and enables accurate calculation of mutation frequencies [3].

In recent years, dPCR has advanced rapidly in the field of rare mutation detection [4]. Researchers have conducted extensive studies on sample adaptation, experimental workflows, and detection methodologies. Novel droplet dPCR platforms have been developed for mutation screening and measurable residual disease monitoring in acute myeloid leukemia [5]. Other studies have optimized detection strategies for challenging sample types including formalin-fixed paraffin-embedded tissues and circulating free DNA. These efforts have helped overcome issues related to nucleic acid degradation and inhibitor interference [6]. In parallel, machine learning techniques have gradually been introduced into dPCR data analysis. Algorithms such as support vector machines and random forests have been applied to improve droplet classification performance [7]. These advances have promoted the clinical translation of dPCR in oncology, hematological disorders, and other medical fields [8]. Despite these achievements, several limitations remain in current dPCR technologies [9]. Conventional clustering algorithms including K-means and Gaussian mixture models are highly susceptible to matrix interference from clinical samples, fluorescence signal overlap, and nonspecific amplification. These factors often result in droplet misclassification [10]. Existing machine learning approaches typically focus only on droplet clustering and overlook the influence of critical experimental parameters such as primer concentration, annealing temperature, and droplet generation pressure. Improper parameter settings can reduce signal intensity and compromise droplet stability [11]. Furthermore, single-task models have limited ability to address sample heterogeneity arising from different cancer types and specimen preservation methods. Consequently, their generalization performance is often inadequate for diverse clinical testing scenarios [12]. To date, no study has applied multi-task learning (MTL) to optimize the entire workflow of dPCR-based rare mutation detection.

This study developed a dPCR experimental optimization system for rare mutation detection. The proposed framework was designed to reduce droplet classification errors, minimize dependence on manual parameter tuning, and improve adaptability across diverse clinical scenarios. The system integrated dPCR droplet clustering analysis with MTL framework. Multidimensional fluorescence features were extracted from droplets and subsequently standardized. A model architecture consisting of a shared feature extraction layer and two task-specific branches was then constructed. By combining a constrained K-means objective function with a weighted loss function, the framework achieved collaborative optimization of precise droplet clustering and adaptive experimental parameter adjustment. This study was the first to introduce MTL into the complete workflow of dPCR-based rare mutation detection. A closed-loop optimization framework was established to link droplet characteristics with experimental parameters. The proposed approach improved the sensitivity, specificity, and reproducibility of rare mutation detection and facilitated the standardized application of dPCR in complex clinical samples. Furthermore, the study provided new methodological insights for precision oncology and the early diagnosis of infectious diseases.

Materials and methods

Overall system architecture and experimental workflow

The proposed system was designed to achieve closed-loop collaborative optimization of precise droplet clustering and adaptive experimental parameter regulation through deep mining of droplet fluorescence characteristics within MTL framework [13]. The architecture consisted of three major modules including hardware execution, dual-task modeling, and dynamic feedback. Together, these modules ensured high sensitivity and stability in rare mutation detection [14]. The dPCR workflow comprised a sequence of automated procedures including droplet image denoising, multidimensional feature extraction, feature standardization,

multitask model computation, and dynamic parameter feedback. These processes formed a complete automated optimization pipeline for dPCR-based rare mutation detection. The system conducted image denoising for the droplet image obtained after dPCR amplification [15], and then extracted multiple features to construct a feature vector as follows [16].

$$X = [I, A, k, \text{SNR}, \delta, R]^T \quad (1)$$

where *I* was the fluorescence intensity. *A* was fluorescence area. *k* was signal rising slope. SNR was signal-to-noise ratio. δ was fluorescence decay coefficient. *R* was droplet roundness. The SNR was used to quantify the relative intensity of effective droplet fluorescence signals against background noise and served as an important indicator of signal quality. The δ reflected the stability of the fluorescence signal over time and was the ratio of late to early fluorescence intensity as shown below.

$$\delta = \frac{I_{\text{late}}}{I_{\text{early}}} \quad (2)$$

Droplet roundness (*R*) was used to find valid droplets and exclude invalid ones (broken or fused) and was calculated as below.

$$R = \frac{4\pi A}{L^2} \quad (3)$$

where *L* was the contour perimeter of the droplet [17]. Fluorescence SNR was calculated by a local background differential method as shown below.

$$\text{SNR} = \frac{max(I) - \bar{I}_b}{\sigma_{I_b}} \quad (4)$$

where $max(I)$ was the maximum droplet fluorescence intensity. $\bar{I}_b$ was the mean background fluorescence. σ_{I_b} was the background signal standard deviation [18]. To normalize features to the same scale, the Z-score normalization of feature vectors was performed as follows.

$$X_i^* = \frac{X_i - \mu_i}{\sigma_i} \quad (5)$$

where μ_i and σ_i were the mean and standard deviation of the *i*-th feature, respectively [19]. The main MTL framework contained a common feature extraction component and two particular branches of droplet clustering and experimental parameter optimization [20]. The common feature extractor took on the cross-task similarities by means of a nonlinear process as follows.

$$h = \tanh(W_s X^* + b_s) \quad (6)$$

where $W_s \in \mathbb{R}^{d \times 6}$ was the shared weight matrices. $b_s \in \mathbb{R}^d$ was the bias vectors. *d* was the shared feature dimension. tanh enhanced feature representation [21]. The droplet clustering branch used task-specific parameters to map features into a probability over classes as positive, negative, ambiguous as shown below.

$$P(c|h) = \text{Softmax}(W_c h + b_c) \quad (7)$$

where $W_c \in \mathbb{R}^{3 \times d}$ and $b_c \in \mathbb{R}^3$ were branch-specific parameters [22]. To increase clustering resilience, a constrained K-means objective was used. The correlation constraint between shared features and cluster centers was included as follows.

$$J_c = \sum_{n=1}^{N} \sum_{k=1}^{3} \gamma_{nk} \| h_n - \mu_k \|^2 + \lambda \sum_{k=1}^{3} \mu_k^T W_s W_s^T \mu_k \quad (8)$$

where γ_{nk} was the indicator variable (γ_{nk}= 1 if the *n*-th droplet belonged to the *k*-th cluster). μ_k was a centroid of a cluster. λ was a constraint coefficient [23]. The cluster centroid was updated as follows.

$$\mu_k = \frac{\sum_{n=1}^{N} \gamma_{nk} h_n}{\sum_{n=1}^{N} \gamma_{nk}} \quad (9)$$

The experimental parameter optimization branch output was the best possible combination for primer concentration (C_p), annealing temperature (T_a), and droplet generation-pressure (*P*) as below.

$$[\hat{C}_p, \hat{T}_a, \hat{P}] = W_p h + b_p + \varepsilon \quad (10)$$

where $W_p \in \mathbb{R}^{3\times d}$ and $b_p \in \mathbb{R}^3$ were branch-specific parameters. $\varepsilon \sim N(0, \sigma_\varepsilon^2)$ was a stochastic perturbation to avoid local optima [24]. The clustering loss of cross-entropy was used as shown below.

$$L_c = -\sum_{n=1}^{N}\sum_{k=1}^{3} y_{nk} \log P(c_k|h_n) \quad (11)$$

where y_{nk} was the true class label of the n-th droplet [25]. The parameter optimization loss used a weighted mean squared error to increase the weight of important parameters such as annealing temperature as shown below.

$$L_p = \sum_{t=1}^{3} \omega_t \cdot \frac{1}{M}\sum_{m=1}^{M}(\hat{\theta}_{mt} - \theta_{mt}^*)^2 \quad (12)$$

where ω_t was the parameter weights ($\sum_{t=1}^{3}\omega_t = 1$). $\hat{\theta}_{mt}$ was the predicted parameter. θ_{mt}^* was the best validated parameter. *M* was the sample size [26]. MTL loss summed together the losses of the two tasks with adaptive weighting as shown below.

$$L_{\text{total}} = \frac{L_c}{L_c^{\max}} \cdot \alpha + \frac{L_p}{L_p^{\max}} \cdot (1-\alpha) \quad (13)$$

where $L_c^{\max}$ and $L_p^{\max}$ were the losses of the model at which it reached its maximum during training. α was an adaptive weight based on the ratio between the task loss and the total loss [27]. Model parameters were updated by the Adam optimizer with an exponential decay rate as follows.

$$\eta_t = \eta_0 \cdot \exp(-\gamma t) \quad (14)$$

$$\Theta = \Theta - \eta_t \nabla_\Theta L_{\text{total}} \quad (15)$$

where $\Theta = W_s, b_s, W_c, b_c, W_p, b_p\}$ were the trainable parameters. η_0 was the initial learning rate. *γ* was a decreasing factor. *t* was the iteration step [28]. The system output the best experimental parameters and droplets and continuously classified them into droplet groups by outputting best experimental parameters in a loop of "parameters adjustment - amplification-clustering", which greatly improved the rare mutation detection performance in complex samples [29]. The MTL model consisted of three components including a shared feature extraction module, a droplet clustering branch, and an experimental parameter optimization branch. The shared feature extraction module employed fully connected layers with the hyperbolic tangent (tanh) activation function and accepted input data with a dimension of 32 × 6. Both the droplet clustering branch and the experimental parameter optimization branch adopted fully connected architectures with dimensions of 3 × 32 and 3 × 32, respectively. The clustering branch generated classification results through a Softmax function, whereas the parameter optimization branch used a linear output layer. The model contained approximately 2,100 trainable parameters in total. The proposed MTL framework operated in a closed-loop manner consisting of feature extraction, dual-task collaborative optimization, parameter feedback, and experimental iteration, which enabled dynamic regulation of the dPCR system. The shared module first extracted task-related representations from droplet signals. The two task-specific branches then performed droplet classification and experimental parameter optimization in parallel. The optimized parameters were fed back into the experimental process to support iterative refinement. The shared feature extraction layer captured multidimensional features from droplet fluorescence signals [30]. These features were processed in two ways. First, they were fed into the droplet clustering branch to classify positive, negative, and ambiguous droplets with high precision. Second, they were sent to the parameter optimization branch, which output the optimal experimental parameter set [31]. This parameter set directly controlled the experimental process *via* the dPCR instrument's custom interface, compatible with the hardware protocols of Bio-Rad QX200 (Bio-Rad, Hercules, California, USA) and Thermo Fisher QuantStudio 3D (Thermo Fisher, Richardson, Texas, USA)

digital PCR instruments. Primer concentrations were adjusted in real time using Eppendorf epMotion 5075 high-precision automatic pipetting system (Eppendorf AG, Hamburg, Germany) with error 0.1 μM to prevent nonspecific amplification [32]. Annealing temperatures were calibrated by the thermal cycling module of the PCR instrument with accuracy ±0.1°C to match the amplification efficiency of different mutation sites. Droplet generation pressure was controlled dynamically through a pressure regulation valve ranged 0.3 - 0.8 MPa to optimize droplet uniformity. The classification results from the clustering branch were quantified by a feedback module into parameter adjustment weights based on an adaptive coefficient α derived from cross-entropy loss. When clustering accuracy fell below 95%, the system increased the weight loss of the parameter optimization branch (α reduced to 0.3), prioritizing the correction of experimental conditions. When accuracy reached or exceeded 95%, α was maintained at 0.5 to ensure balanced improvement in both tasks. The core of this closed-loop mechanism was the intrinsic mapping between droplet signal features and experimental parameters. Parameter optimization proceeded gradually using an Adam optimizer with an exponential decay of the learning rate. The Adam optimizer used in the model training of this study was implemented based on the PyTorch framework (https://docs.pytorch.org/docs/stable/generated/torch.optim.adam.html). The optimizer was an adaptive moment estimation optimization algorithm and could dynamically adjust the learning rate and ensure the efficient convergence of the model, which formed a positive feedback cycle as parameter adjustment → improved amplification efficiency → higher clustering accuracy → further parameter optimization [33]. For droplet generation pressure control in the Bio-Rad dPCR system, the Swagelok S series precision adjustable valve (Swagelok, Solon, Ohio, USA) replaced original pressure valve with an accuracy of ±0.01 MPa. Nitrogen pressure was regulated with a knob-operated adjustment rod. The pressure range was 0.4 - 0.7 MPa with step increments of 0.02 MPa. The automated DG module used Bio-Rad's OpenApi software development kit. A Python script called the instrument's pressure control interface and modified internal register parameters with address at 0x0028 to automate droplet generation pressure adjustment. The whole set of pressure control components could realize the fine and step-by-step adjustment of droplet generation pressure and ensure the stable output of experimental pressure parameters. The mapping between script parameters and pressure values followed a linear calibration equation as below [34].

$$\hat{P} = 0.003 \times \text{Param} + 0.38 \ (R^2 = 0.997) \qquad (16)$$

Droplet generation efficiency (≥95%) and uniformity (CV ≤2.1%) met experimental requirements. To determine the fluorescence decay coefficient (δ) under endpoint reading mode, individual droplets were first segmented using Otsu thresholding combined with morphological operations (dilation-erosion). Binary masks were obtained for each droplet region. Based on the droplet's geometric center, each droplet was divided into a central region with radius as 1/2 of total droplet radius (early signal region) and a peripheral region, the ring outside the center (late signal region). This division reflected the diffusion characteristics of fluorescent molecules after PCR amplification. The central region had high, stable fluorescence, whereas the peripheral region had lower intensity and noticeable decay. The average fluorescence intensity of the central region was designated as I_{early}, and that of the peripheral region as I_{late}. The decay coefficient was calculated as $\delta = I_{\text{late}}/I_{\text{early}}$. Fluorescence microsphere standards (Thermo Fisher F8810, 1 μm diameter) were used for intensity calibration to ensure consistency across instruments (CV ≤1.8%) [35]. Measured decay coefficients correlated strongly with real-time quantitative PCR decay rates (R^2 = 0.982), satisfying methodological requirements.

Droplet feature extraction and calculation

The ground-truth droplet labels (positive, negative, or ambiguous) were determined using a three-tier validation strategy. The next-generation sequencing (NGS) results were used as the first tier. A droplet was labeled positive if the variant allele frequency (VAF) at the mutation site was ≥ 0.1% with sequencing coverage ≥ 1,000×, and negative if VAF = 0. In the second tier, ambiguous droplets (0 < VAF < 0.1%) were verified using Sanger sequencing. A droplet was labeled positive if the signal intensity at the target mutation site in the electropherogram exceeded three times the background signal. Otherwise, it was labeled negative. In the third tier, the assigned labels were validated through repeated dPCR experiments (n = 3). A droplet label was finalized only if the signal consistency across the three experiments was ≥ 98%, excluding random errors that could produce false positives or negatives. The concordance of labels across validation methods was assessed using the Kappa coefficient. A Kappa ≥ 0.85 was considered valid.

MTL model construction

Bio-Rad QuantaSoft (v1.7.4) was applied for droplet classification with the mean ± 2 standard deviations. In contrast, the MTL system used a dynamic fused threshold strategy. An initial threshold range [0.5, 0.7] was determined based on the distances between cluster centers of positive and negative droplets in the training set. Then, the threshold was optimized on the validation set using the Youden index (J = sensitivity + specificity − 1) as the objective function. Grid search with a step size of 0.01 identified the optimal threshold as 0.62 ± 0.03. To adapt to different sample types, sample-specific correction coefficients were applied. The feature extraction workflow included that dPCR droplet images were first denoised using Gaussian filtering (σ = 1.5) and contrast-enhanced with the CLAHE algorithm. Droplet regions were then segmented using Otsu thresholding, and artifacts were removed *via* area filtering (100 - 500 pixels). Fluorescence intensity (mean grayscale of droplet pixels), fluorescence area (number of pixels × pixel area, 1.21 μm²/pixel), and SNR (using a 5-pixel-wide local background region) were extracted. Model training hyperparameters were batch size = 32, training steps = 5,000, Adam optimizer with $\beta_1 = 0.9$, $\beta_2 = 0.999$, weight decay = $1e^{-4}$, and initial adaptive weight $\alpha = 0.5$, updated every 100 iterations. Data preprocessing involved K-nearest neighbor imputation (k = 5) for missing values and Z-score filtering ($|Z| > 3$) for outliers. Stratified random splitting allocated 70% of data to the training set, 15% to the validation set, and 15% to the test set, maintaining balanced distributions of tumor and sample types. Reproducibility was evaluated across three independent Bio-Rad QX200 instruments using the same standard sample (EGFR L858R mutant plasmid, 10^2 copies/μL) in five repeated experiments. The coefficient of variation (CV) of core performance metrics (sensitivity, specificity, clustering accuracy) was required to be ≤ 1.5%, and observed CV ranged from 0.6% to 1.2%. The dPCR reaction mixture (20 μL) consisted of 10 μL 2× ddPCR Supermix, 0.5 μL primer pair (10 μM), 0.2 μL probe (10 μM), 2 μL template DNA, and 7.3 μL nuclease-free water. Thermal cycling program was 95°C for 10 min followed by 40 cycles of 94°C for 30 s, 60°C for 1 min, and final 98°C for 10 min. Droplet generation conditions were set at 0.5 MPa for 2 min.

Data sources

Publicly available datasets that integrated dPCR droplet characteristics with clinical sample information and covered multiple cancer types, sample matrices, mutation targets, and experimental conditions were employed in this study. All samples had been validated using standard methods including NGS with sequencing depth ≥ 1,000× and Sanger sequencing for model training, validation, and performance evaluation. The primary datasets were Sequence Read Archive (SRA) from the National Center for Biotechnology Information (NCBI) with the accession numbers of PRJNA752876 and PRJNA680867. Together, 265 samples covering two cancer types, three mutation targets, and three specimen categories

were included in this study with approximately 1.8 million valid droplets. Additional data were obtained from the ArrayExpress repository of the European Bioinformatics Institute (EBI) under accession number of E-MTAB-10987. Approximately 500,000 valid droplets were included in this dataset. All datasets underwent standardized preprocessing before model development. A droplet circularity threshold of $R \geq 0.8$ was applied to remove damaged, merged, and signal-deficient droplets. Droplet classification labels were corrected according to the clinical validation results reported in the original studies. To address differences between the Bio-Rad QX200 and Thermo Fisher QuantStudio 3D platforms, instrument-specific calibration and normalization procedures were performed. These procedures preserved the original fluorescence distribution patterns and maintained the relationships between droplet features and experimental parameters. After data integration, the final dataset consisted of 337 clinical samples covering six cancer types and eight rare mutation targets. The dataset contained approximately 2.3 million valid droplets and included three specimen categories. Retrieved data were collected using three different dPCR instrument models, thereby providing substantial diversity in experimental conditions. The model parameters were configured as an initial learning rate of 0.001, a learning decay coefficient of 0.0001, a constraint coefficient (λ) of 0.01, and a total of 5,000 training iterations. The parameter weights ω_1, ω_2, and ω_3 were set to 0.3, 0.5, and 0.2, respectively. Collectively, the integrated dataset realistically represented sample characteristics across diverse clinical scenarios and experimental environments, thereby providing a comprehensive and reliable data foundation for droplet clustering optimization and adaptive experimental parameter regulation.

Evaluation of proposed system

To evaluate the generalization capability of the proposed system under clinical conditions, three types of clinical specimens were tested including formalin-fixed paraffin-embedded (FFPE) tissues, circulating cell-free DNA (cfDNA) from plasma, and fresh tumor tissues. Two dPCR platforms, the Bio-Rad QX200 and Thermo Fisher QuantStudio 3D systems, were used for experimental validation. Eight clinically relevant rare mutation sites were selected as detection targets. A unified dPCR reaction system and amplification protocol were applied throughout the study. Parallel analyses were performed across different sample types, mutation targets, and instruments. Detection accuracy was recorded for each experimental group, and both mean values and coefficients of variation (CVs) were calculated. The performance of the proposed system was further compared with commercial dPCR analysis software including Random Forest (RF), Support Vector Machine (SVM), and K-means algorithms for a comprehensive assessment of system stability and generalization under complex clinical conditions. To evaluate the analytical sensitivity of different detection approaches, a series of gradient-diluted EGFR L858R mutant plasmids with concentrations ranging from 0.1 to 10 copies/μL was employed. The limit of detection (LOD) was defined as the lowest plasmid concentration at which the detection success rate reached 95%. In addition, plasma cfDNA samples collected from 100 healthy individuals were used to determine the false-positive rate of a single assay. Standard reference samples with VAFs ranging from 0.1% to 5% were further analyzed to assess VAF quantification accuracy by comparing measured values with theoretical values. A prospective clinical cohort study was conducted between March and December 2024 in the Department of Oncology at Luohe Central Hospital (Luohe, Henan, China). A total of 150 patients with advanced solid tumors were recruited including 82 patients with lung cancer, 45 patients with colorectal cancer, and 23 patients with other tumor types. Clinical specimens consisted of 50 plasma cfDNA samples, 50 FFPE tissue samples, and 50 fresh tumor tissue samples. NGS results generated using the Illumina NovaSeq 6000 platform (Illumina, San Diego, CA, USA) served as the reference standard. All samples underwent standardized preprocessing, dPCR analysis, and

data interpretation procedures. The clinical performance of the proposed system was then systematically evaluated. All study protocols and procedures were approved by the Ethics Committee of Luohe Central Hospital (Luohe, Henan, China).

Statistical analysis

SPSS 26.0 (IBM, Armonk, NY, USA) was used for statistical analysis. Intergroup comparisons were conducted using independent samples *t*-tests. *P* value less than 0.05 was considered statistically significant, whereas *P* value less than 0.001 indicated a highly significant difference. Agreement between detection methods was evaluated using Cohen's Kappa test. Kappa values closer to 1 indicated stronger agreement between different detection approaches.

Results

Validation of proposed system

The concordance of labels across NGS, Sanger sequencing, and repeated dPCR demonstrated overall consistency of 98.7%, positive droplet consistency of 97.9%, and negative droplet consistency of 99.2% with Kappa of 0.92 ± 0.03, ensuring the authority of the ground-truth labels [36]. The performance of the dynamic threshold with the commercial automatic threshold showed that the MTL system achieved a Youden index of 0.957, significantly higher than the commercial software's 0.913 ($P < 0.001$), demonstrating the superiority of this strategy [37]. Sample-specific correction coefficients were applied to adapt to different sample types with FFPE of 1.05, cfDNA of 0.98, and fresh tissue of 1.00. The proposed system achieved an overall clinical concordance rate of 97.3% with a Kappa coefficient of 0.94. In the lung cancer subgroup, the concordance rate reached 98.8% with a Kappa coefficient of 0.97. For colorectal cancer, the concordance rate was 95.6% with a Kappa coefficient of 0.90. Among low-abundance mutation samples with variant allele frequencies below 1%, the concordance rate remained as high as 93.8% with a Kappa coefficient of 0.87. All performance metrics obtained by the commercial software were lower than those achieved by the proposed system with statistically significant difference.

Evaluation of the rare mutation detection experimental optimization system

The main indicators of the system performance showed that the MTL system outperformed both traditional ML systems and commercial software on all the important performance metrics for rare mutation detection. The sensitivity of the MTL system reached 97.2 ± 0.8% and increased by 4.7%, 6.9%, 8.5%, and 12.1% compared to commercial dPCR software (92.5%), random forest (90.3%), SVM (88.7%), and k-means (85.1%). The specificity showed that the MTL achieved 98.5 ± 0.5%, which was ahead of commercial software by 4.2% and K-means by 8.9%, showing its powerful anti-interference ability. The clustering accuracy of the MTL system reached 96.8%, which was up by 5.1% compared to commercial software, thus effectively lowering the risk of mistaking droplets. The parameter optimize adaptable was 0.95, which was much more than the single task model (0.73-0.78) and the traditional algorithm (0.65) (Figure 1). In all cases, the MTL systems had the lowest SDs, which reflected great stability. The results suggested the advantage of integrating droplet clustering and parameter optimization inside the MTL framework, thus successfully addressed the shortfalls of low sensitivity and poor generalization from typical approaches and provided strong technical aid in accurate rare mutation discovery. The results of the analytical sensitivity of different detection approaches demonstrated that the proposed MTL system achieved an LOD of as low as 0.8 ± 0.1 copies/μL. The false-positive rate was only 0.021 ± 0.003 per assay, while the VAF detection accuracy reached 98.3% ± 0.6%, corresponding to a coefficient of variation of 1.1% ± 0.2%. All performance metrics obtained using commercial software and the conventional K-means algorithm were inferior to those achieved by the proposed system ($P < 0.001$). To further evaluate the generalization stability of the proposed framework across

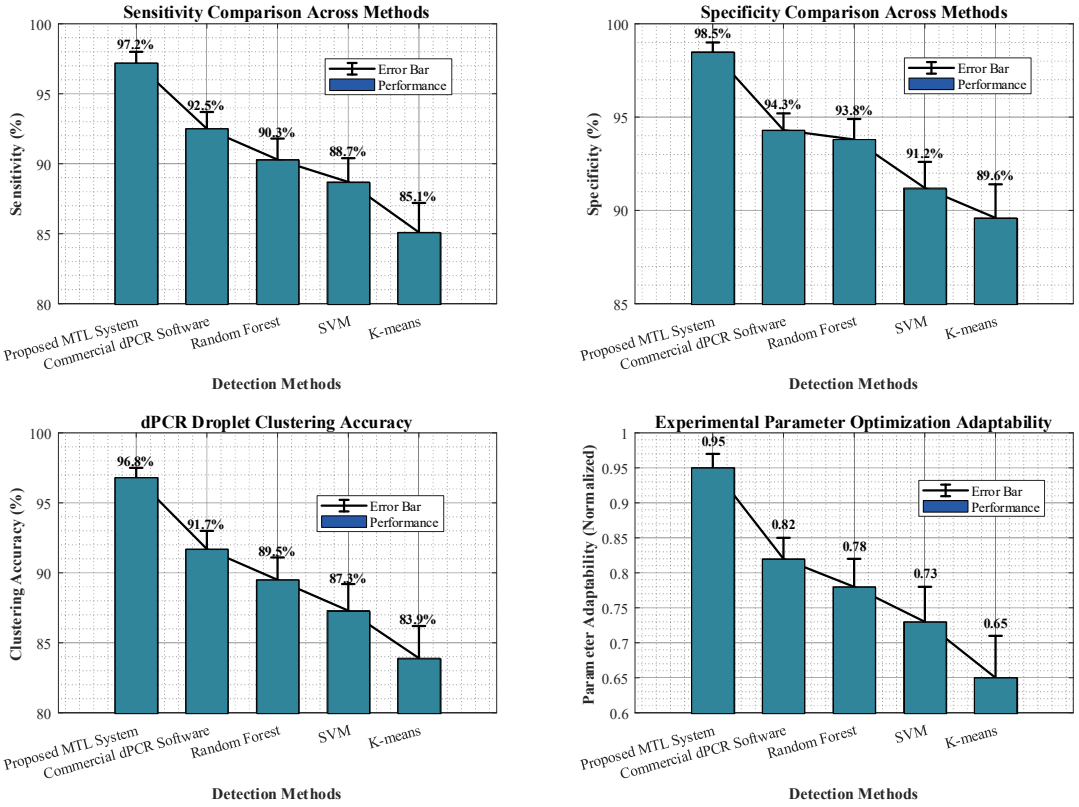

Figure 1. Validation of the system's core performance metrics.

heterogeneous datasets, cross-validation experiments were performed using a leave-one-instrument-out strategy and a leave-one-mutation-site-out strategy. The results showed that the average detection accuracy ranged from 95.1% to 96.3%, and the coefficient of variation remained between 1.0% and 1.5%. No statistically significant differences were observed when compared with stratified random data partitioning. The findings indicated that the characteristics associated with a specific instrument platform or mutation target did not substantially affect system performance. The proposed framework effectively addressed the limitations of conventional validation approaches when applied to heterogeneous datasets. Compared with standard random-split validation methods, the adopted cross-validation strategies more closely reflected real-world clinical deployment scenarios. The results therefore provided strong evidence that the MTL framework possessed excellent generalization capability across multiple dPCR platforms and mutation targets, supporting its future clinical translation and standardized implementation.

Evaluation of clinical scenario generalizability

The results of the clinical scenario generalizability evaluation showed that the proposed MTL system had good stability and adaptability to complex clinical variables. Sample matrix performance demonstrated that the MTL systems reached 95.3% for FFPE, 97.8% for cfDNA, and 98.1% for fresh tissues, all above those of commercial software (88.6 - 93.7%), while the standard deviation also decreased from 1.0 - 1.8% to 0.5 - 1.1%, meaning that it could overcome interference due to nucleic acid degradation in FFPE samples. Instrument compatibility showed that the results were consistent across Bio-Rad QX200 (96.5%) and Thermo Fisher QuantStudio 3D (95.9%), beating random forest (87.6 - 88.9%) and SVM (84.4 - 85.6%) by 8 - 11%. Mutation coverage showed

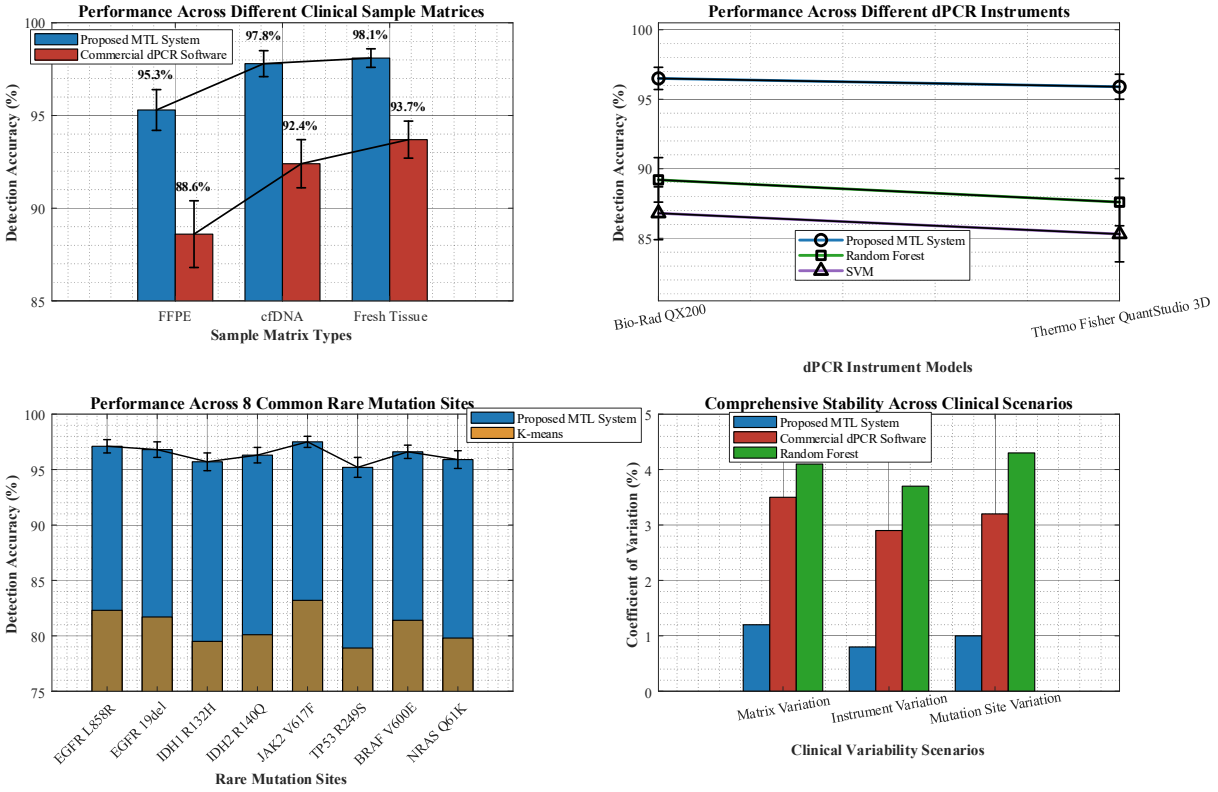

Figure 2. Clinical scenario generalizability assessment results.

that, for the eight rare mutations, MTL retained accuracy range of 95.2 - 97.5%, which was higher than K-means' range of 78.9 - 83.2%. Robustness indicated that the system's CV was only 0.8 - 1.2% much lower than the commercial software (2.9 - 3.5%) and random forest (3.7 - 4.3%), proving its ability to have strong generalization on diverse clinical situations (Figure 2).

Prospective clinical validation

The results of the prospective wet-lab validation demonstrated that the proposed dPCR rare mutation detection optimization system based on droplet clustering and MTL had effectively solved the problems of large classification error of traditional algorithms and dependence of experimental parameters on manual experience. The detection limit of the system was as low as 0.8 ± 0.1 copies/μL. The key indicators such as false positive rate and frequency accuracy of mutant alleles were significantly better than those of commercial software, traditional K-means, support vector machine, and random forest algorithm (Table 1). Meanwhile, it was stable in cross-validation of multi-instrument and multi-mutation sites, which proved that the framework had excellent detection performance and data heterogeneous adaptation ability.

Discussion

The study provided a brand-new automatic analysis scheme for accurate molecular diagnosis of tumors. A closed-loop system for the optimization of rare mutation detection experiments based on droplet clustering analysis and multi-task learning was constructed in this study to solve the key bottlenecks in the existing technology of digital PCR such as droplet classification being easily interfered by sample matrix, overlapping fluorescence signals, highly dependent on manual debugging of experimental parameters, and insufficient

Table 1. Prospective wet-lab validation results.

Experimental group	Parameter settings	Amplification efficiency (%)	Fluorescence signal intensity	Positive droplet recognition rate (%)	Detection success rate (%)
MTL-recommended parameters	Primer: 0.35 μM Annealing: 61.2 °C Droplet generation pressure: 52 MPa	98.7 ± 0.5	1286 ± 32	97.6 ± 0.8	99.3
Predefined experimental scheme	Primer: 0.5 μM Annealing: 60°C Droplet generation pressure: 0.5 MPa	91.3 ± 1.2	968 ± 45	90.2 ± 1.5	92.7
P value (group comparison)	-	< 0.001	< 0.001	< 0.001	< 0.001

clinical generalization ability of single-task model. Based on the integration of NCBI and EBI public databases, standardized datasets covering 6 types of tumors, 8 types of rare clinical mutations, 3 types of clinical samples (FFPE tissue, plasma free DNA, fresh tumor tissue), and nearly 2.3 million effective droplets were obtained to complete the model training and verification. The performance test results showed that the sensitivity of rare mutation detection in this proposed system was 97.2%, the specificity was 98.5%, and the accuracy of droplet clustering was 96.8%. Compared with commercial QuantaSoft software, random forest, support vector machine, and traditional K-means algorithm, the performance of proposed system was improved significantly (P < 0.001). The detection limit, the false positive rate of single reaction, the quantitative accuracy of mutant allele frequency, and the coefficient of variation of each index of the proposed system were all superior over the existing analysis tools, while the ability of resisting sample degradation and non-specific amplification interference were also outstanding. The cross-validation results showed that the detection accuracy of the model was stable at high percentages under different detection platforms and mutation sites with no significant performance degradation. It had excellent cross-equipment and cross-target generalization ability. A single-center prospective clinical cohort study with patients diagnosed advanced solid tumors and NGS sequencing as the gold standard showed that the overall clinical detection coincidence rate of proposed system was 97.3% with Kappa coefficient of 0.94. The lung cancer samples showed the highest coincidence degree. The coincidence degree of low-abundance mutation (VAF < 1%) samples still reached high value and significantly better than that of commercial analysis software to stably meet the needs of clinical low-abundance rare mutation screening. The hierarchical verification results showed that the detection accuracy of the proposed system was stable above 95% for all types of samples tested. The dynamic fusion threshold combined with sample type correction coefficient effectively compensated for the sample adaptation defects of the traditional fixed threshold algorithm. In this study, multi-task learning was completely embedded into the whole process of digital PCR for rare mutation detection for the first time, which broke through the internal relationship between the fluorescence characteristics of droplets and experimental control parameters, got rid of the dependence of traditional analytical tools on manual experience parameter adjustment, and greatly reduced the clinical detection pain points such as droplet misclassification, false positive, and quantitative deviation. The hardware transformation scheme of the whole system was universal, and the algorithm framework was portable. It was compatible with mainstream commercial dPCR instruments, while the operation process was highly automated with no

need of complex manual intervention. Therefore, the proposed system could adapt to various clinical diagnosis and treatment scenarios such as early screening of tumors, monitoring of drug-resistant mutations, and evaluation of minimal residual lesions. However, there were still some limitations in this study. The sample source of the validation cohort was single. Multi-center and large-sample clinical research were needed to further verify the clinical transformation value of the system. The model was only trained for 8 rare mutations of high-frequency tumors, and the mutation site database could be expanded to more molecular diagnosis scenarios such as hematological diseases and infectious diseases in the future. The dPCR experimental optimization system based on multi-task learning and droplet clustering proposed in this research effectively overcame the shortcomings of traditional digital PCR technology standardization application, provided stable, highly sensitive, and repeatable automatic technical support for accurate tumor detection, and had important clinical transformation and *in vitro* diagnosis standardization promotion value.

Acknowledgements

This work was supported by 2022 Henan Provincial Vocational Education Teaching Reform Research and Practice Project.

References

1. Wu Z, Yao W, Chen J, Chen Y, Li Z, Ding W, *et al*. 2025. Droplet digital PCR-based single aptamer selection. Talanta. 292:127924.
2. Chen X, Liu L, Zhang A, Yi M, Lan Y, Zheng Z, *et al*. 2022. Droplet digital PCR for genetic mutations monitoring predicts relapse risk in pediatric acute myeloid leukemia. Int J Hematol. 116(5):669-677.
3. Sawakwongpra K, Tangmansakulchai K, Ngonsawan W, Promwan S, Chanchamroen S, Quangkananurug W, *et al*. 2021. Droplet-based digital PCR for non-invasive prenatal genetic diagnosis of α and β-thalassemia. Biomed Rep. 15(4):82.
4. Callens C, Bidard FC, Curto-Taribo A, Trabelsi-Grati O, Melaabi S, Delaloge S, *et al*. 2022. Real-time detection of ESR1 mutation in blood by droplet digital PCR in the PADA-1 trial: Feasibility and cross-validation with NGS. Anal Chem. 94(16):6297-6303.
5. Galimberti S, Balducci S, Guerrini F, Del Re M, Cacciola R. 2022. Digital droplet PCR in hematologic malignancies: A new useful molecular tool. Diagnostics. 12(6):1305.
6. Ren J, Xu G, Liu H, He N, Zhao Z, Wang M, *et al*. 2023. A chamber-based digital PCR based on a microfluidic chip for the absolute quantification and analysis of KRAS mutation. Biosensors. 13(8):778.
7. Paolis E, De Bonis M, Concolino P, Piermattei A, Fagotti A, Urbani A, *et al*. 2021. Droplet digital PCR for large genomic rearrangements detection: A promising strategy in tissue BRCA1 testing. Clin Chim Acta. 513:17-24.
8. Li Y, Tan G, Zhou Y. 2022. Digital PCR and its applications in noninvasive prenatal testing. Brief Funct Genomics. 21(5):376-386.
9. Trouchet A, Gines G, Benhaim L, Taly V. 2025. Digital PCR: From early developments to its future application in clinics. Lab Chip. 25(16):3921-3961.
10. Rausch C, Rothenberg-Thurley M, Buerger S A, Tschuri S, Dufour A, Neusser M, *et al*. 2021. Double drop-off droplet digital PCR: A novel, versatile tool for mutation screening and residual disease monitoring in acute myeloid leukemia using cellular or cell-free DNA. J Mol Diagn. 23(8):975-985.
11. Carvalho TM, Dourado RM, Nakatani SM, Duarte CAB, Ioshii SO, Riediger IN, *et al*. 2021. Digital PCR detection of EGFR somatic mutations in non-small-cell lung cancer formalin fixed paraffin embedded samples. Mol Cell Probes. 58:101745.
12. Wolter M, Felsberg J, Malzkorn B, Kaulich K, Reifenberger G. 2022. Droplet digital PCR-based analyses for robust, rapid, and sensitive molecular diagnostics of gliomas. Acta Neuropathol Commun. 10(1):42.
13. Shirai R, Osumi T, Keino D, Nakabayashi K, Uchiyama T, Sekiguchi M, *et al*. 2023. Minimal residual disease detection by mutation-specific droplet digital PCR for leukemia/lymphoma. Int J Hematol. 117(6):910-918.
14. Pablo-Fontecha V, Hernández-Illán E, Reparaz A, Asensio E, Morata J, Tonda R, *et al*. 2023. Quantification of rare somatic single nucleotide variants by droplet digital PCR using SuperSelective primers. Sci Rep. 13(1):18997.
15. Hu L, Ji YY, Zhu P, Lu RQ. 2024. Mutation-selected amplification droplet digital PCR: A new single nucleotide variant detection assay for TP53R249S mutant in tumor and plasma samples. Anal Chim Acta. 1318:342929.
16. Liu Y, Han C, Li J, Xu S, Xiao Z, Guo Z, *et al*. 2024. Laboratory-developed droplet digital PCR assay for quantification of the JAK2V617F mutation. Glob Med Genet. 11(02):132-141.
17. Di J, Sheng T, Arora R, Stocks-Candelaria J, Wei S, Lutz C, *et al*. 2025. The validation of digital PCR-based minimal residual disease detection for the common mutations in IDH1 and IDH2 genes in patients with acute myeloid leukemia. J Mol Diagn. 27(2):100-108.
18. Tak LJ, Shin MK, Yoo JI, Cho MC, Kim W. 2023. Development of droplet digital PCR-based detection of bacterial pathogens in prosthetic joint infection: A preliminary study using a synthesized model plasmid. Front Cell Infect Microbiol. 13:1301446.

19. Ntzifa A, Kotsakis A, Georgoulias V, Lianidou E. 2021. Detection of EGFR mutations in plasma cfDNA and paired CTCs of NSCLC patients before and after osimertinib therapy using crystal digital PCR. Cancers. 13(11):2736.
20. Xu J, Wu W, Wu C, Mao Y, Qi X, Guo L, *et al*. 2021. A large-scale, multicentered trial evaluating the sensitivity and specificity of digital PCR versus ARMS-PCR for detecting ctDNA-based EGFR p. T790M in non-small-cell lung cancer patients. Transl Lung Cancer Res. 10(10):3888.
21. Cusenza VY, Bisagni A, Rinaldini M, Cattani C, Frazzi R. 2021. Copy number variation and rearrangements assessment in cancer: Comparison of droplet digital PCR with the current approaches. Int J Mol Sci. 22(9):4732.
22. Bao X, Qin D, Ma J, Zhou X, Wang J, Yao C, *et al*. 2022. Accurate detection of α-globin gene copy number variants with two reactions using droplet digital PCR. Hematology. 27(1):198-203.
23. Nell RJ, Versluis M, Menger NV, Gelmi MC, Vu THK, Verdijk RM, *et al*. 2025. Digital PCR-based genetic profiling from vitreous fluid as liquid biopsy for primary uveal melanoma: A proof-of-concept study. J Exp Clin Cancer Res. 44(1):124.
24. Wainman LM, Sathyanarayana SH, Lefferts JA. 2024. Applications of digital polymerase chain reaction (dPCR) in molecular and clinical testing. J Appl Lab Med. 9(1):124-137.
25. Young FP, Becker TM, Nimir M, Opperman T, Chua W, Balakrishnar B, *et al*. 2022. Biomarkers of castrate resistance in prostate cancer: Androgen receptor amplification and T877A mutation detection by multiplex droplet digital PCR. J Clin Med. 11(1):257.
26. Mana AF, Culp K, Keeler A, Perrera O, Rajagopalan M, Jacky L, *et al*. 2024. Performance of a rapid digital PCR test for the detection of non-small cell lung cancer (NSCLC) variants. Mol Diagn Ther. 28(6):791-802.
27. Sharma NS, Nataraj KS, Choudhary B. 2025. Prevalence, detection, and clinical implications of BRAF V600E and NRAS Q61R mutations in multiple myeloma BM-FFPE tissues using digital droplet PCR. Med Oncol. 42(11):478.
28. Addamo-De Nard B, Geissmann M, Akhoundova D, Pistoni C, Brezina T, Zoche M, *et al*. 2025. A novel KRAS exon 2 drop-off digital PCR assay for mutation detection in cell-free DNA of cancer patients. Diagn Pathol. 20(1):62.
29. Henriksen TV, Drue SO, Frydendahl A, Demuth C, Rasmussen MH, Reinert T, *et al*. 2022. Error characterization and statistical modeling improves circulating tumor DNA detection by droplet digital PCR. Clin Chem. 68(5):657-667.
30. Olmedillas-López S, Olivera-Salazar R, García-Arranz M, García-Olmo D. 2022. Current and emerging applications of droplet digital PCR in oncology: An updated review. Mol Diagn Ther. 26(1):61-87.
31. Mannina D, Badbaran A, Wolschke C, Klyuchnikov E, Christopeit M, Fehse B. 2022. Digital-droplet PCR assays for IDH, DNMT3A and driver mutations to monitor after allogeneic stem cell transplantation minimal residual disease of myelofibrosis. Bone Marrow Transplant. 57(3):510-512.
32. Li B, Liu J, Huang Q. 2023. A digital PCR method based on highly specific Taq for detecting gene editing and mutations. Int J Mol Sci. 24(17):13405.
33. Wu YM, Tang FY, Qi ZX. 2025. Multimodal artificial intelligence technology in the precision diagnosis and treatment of gastroenterology and hepatology: Innovative applications and challenges. World J Gastroenterol. 31(38):109802.
34. Elomaa P, Ojalehto T, Kumar D, Jokinen V, Saavalainen P. 2024. Manually pressurized droplet digital PCR chip for rapid SARS-CoV-2 diagnostics. Biomicrofluidics. 18(1):84-97.
35. Gest AMM, Sahan AZ, Zhong Y, Lin W, Mehta S, Zhang J. 2024. Molecular spies in action: Genetically encoded fluorescent biosensors light up cellular signals. Chem Rev. 124(22):12573-12660.
36. Lord SJ, Horvath AR, Sandberg S, Monaghan PJ, Cobbaert C, Reim M, *et al*. 2025. Is this test fit-for-purpose? Principles and a checklist for evaluating the clinical performance of a test in the new era of *in vitro* diagnostic (IVD) regulation. Crit Rev Clin Lab Sci. 62(3):182-197.
37. Shoop WK, Gorsuch CL, Bacman SR, Moraes CT. 2022. Precise and simultaneous quantification of mitochondrial DNA heteroplasmy and copy number by digital PCR. J Biol Chem. 298(11):102574.